Cascade discrete memristive maps for enhancing chaos

Fang Yuan(袁方), Cheng-Jun Bai(柏承君), and Yu-Xia Li(李玉霞)
Citation: Chin. Phys. B, 2021, 30 (**12**): 120514. DOI: 10.1088/1674-1056/ac20c7
Journal homepage: http://cpb.iphy.ac.cn; http://iopscience.iop.org/cpb

What follows is a list of articles you may be interested in

Controlling chaos and supressing chimeras in a fractional-order discrete phase-locked loop using impulse control

Karthikeyan Rajagopal, Anitha Karthikeyan, and Balamurali Ramakrishnan
Chin. Phys. B, 2021, 30 (**12**): 120512. DOI: 10.1088/1674-1056/ac1b83

Embedding any desired number of coexisting attractors in memristive system

Chunbiao Li(李春彪), Ran Wang(王然), Xu Ma(马旭), Yicheng Jiang(姜易成), and Zuohua Liu(刘作华)
Chin. Phys. B, 2021, 30 (**12**): 120511. DOI: 10.1088/1674-1056/ac1e1f

Acoustic wireless communication based on parameter modulation and complex Lorenz chaotic systems with complex parameters and parametric attractors

Fang-Fang Zhang(张芳芳), Rui Gao(高瑞), and Jian Liu(刘坚)
Chin. Phys. B, 2021, 30 (**8**): 080503. DOI: 10.1088/1674-1056/ac0905

Control of chaos in Frenkel-Kontorova model using reinforcement learning

You-Ming Lei(雷佑铭) and Yan-Yan Han(韩彦彦)
Chin. Phys. B, 2021, 30 (**5**): 050503. DOI: 10.1088/1674-1056/abd74f

A multi-directional controllable multi-scroll conservative chaos generator: Modelling, analysis, and FPGA implementation

En-Zeng Dong(董恩增), Rong-Hao Li(李荣昊), and Sheng-Zhi Du(杜升之)
Chin. Phys. B, 2021, 30 (**2**): 020505. DOI: 10.1088/1674-1056/abc239

SPECIAL TOPIC — Interdisciplinary physics: Complex network dynamics and emerging technologies

Cascade discrete memristive maps for enhancing chaos*

Fang Yuan(袁方)†, Cheng-Jun Bai(柏承君), and Yu-Xia Li(李玉霞)

College of Electrical Engineering and Automation, Shandong University of Science and Technology, Qingdao 266590, *China*

(Received 8 July 2021; revised manuscript received 16 August 2021; accepted manuscript online 25 August 2021)

Continuous-time memristor (CM) has been widely used to generate chaotic oscillations. However, discrete memristor (DM) has not been received adequate attention. Motivated by the cascade structure in electronic circuits, this paper introduces a method to cascade discrete memristive maps for generating chaos and hyperchaos. For a discrete-memristor seed map, it can be self-cascaded many times to get more parameters and complex structures, but with larger chaotic areas and Lyapunov exponents. Comparisons of dynamic characteristics between the seed map and cascading maps are explored. Meanwhile, numerical simulation results are verified by the hardware implementation.

Keywords: chaos, discrete memristor, cascade chaotic system, bifurcation

PACS: 05.45.–a, 05.45.Pq, 84.32.–y **DOI:** 10.1088/1674-1056/ac20c7

1. Introduction

Memristor, as the fourth basic circuit component, has some special characteristics, such as inherent nonlinearity and synaptic plasticity. According to the mathematical models, memristors can be classified into extended memristor, generic memristor, and ideal memristor.[1] Different memristors exhibit different properties. Since the unique characteristics of memristors, chaotic circuits,[2–4] neuromorphic computing systems[5–7] and other nonlinear systems[8,9] used to describe many problems in the fields of biology, physics, and economics can be easily constructed by combining memristors with other devices, which makes memristors be applied broadly in a potential application prospect.

Chaotic and hyperchaotic behaviors can be found in continuous and discrete nonlinear dynamical systems,[10–17] which have many unique behaviors, including topological transitivity, initial state sensitivity, and periodic orbit density.[18–21] In order to obtain new chaotic systems with rich repertoires of nonlinear behaviors, memristors were introduced into some classical chaotic circuits.[22–25] In addition, a cascade method of forming a series of new systems by cascading two chaotic subsystems was proposed in our previous papers.[26,27] Theoretical verification and experimental results manifested that the Lyapunov exponents and chaotic space of the new cascade chaotic system are much larger than those of subsystems.

As we all know, systems can be classified into continuous systems and discrete systems. Memristor is not an exception. Chua proposed that the concept of memristor can be extended to a much more general class of dynamical systems called memristive systems (or generalized memristors), and the memristor is only a special case of the systems.[28] Compared with CM-based systems, DM-based systems can be naturally realized by digital platforms such as FPGA (field programmable gate array), DSP (digital signal processing), and other microprocessor platforms. Besides, discrete systems can be utilized to appropriately describe many complex problems in the real world. Hence, the DM and DM-based systems may have many potential applications. Based on this idea, some DMs have been proposed in recent years.[29–31] For example, in Ref. [32], He *et al.* investigated a DM model which are applied to the Hénon map. The bifurcation diagram and Lyapunov exponents were studied. The simulation results confirmed that the new DM-based map has more complexities than the original Hénon map. What is more, Bao *et al.* proposed a new discrete hyperchaotic map, which was from a sampling switch-based memristor-based circuit.[33] Inspired by this work, a general DM model and its mapping model were reported in Ref. [34]. Based on the DM mapping model, four different DM models and their maps were provided. The excellent performances indicated that two of the DM mappings can generate hyperchaos and show the memristor initial-boosted behaviors. In addition to the ideal DM model, a simple two-dimensional (2D) non-autonomous DM-based hyperchaotic map was proposed by Deng, which shows the bursting behaviors.[35] The above DM models and mappings all indicate that designing a chaotic discrete map with more complexities and better performances is still a valuable research topic.

*Project supported by the National Natural Science Foundation of China (Grant Nos. 61801271, 61973200, and 91848206), the Natural Science Foundation of Shandong Province, China (Grant No. ZR2019BF007), the Qingdao Science and Technology Plan Project (Grant No. 19-6-2-9-cg), the Elite Project of Shandong University of Science and Technology, the Taishan Scholar Project of Shandong Province of China, and the Scientific Research Foundation of Shandong University of Science and Technology for Recruited Talents.

†Corresponding author. E-mail: yf210yf@163.com

Encouraged by the above examples, the main contents of this paper can be introduced as follows. The DM chaotic map (DMCM) is first used as a seed map to construct new cascade systems (CSs). To demonstrate the cascade method, the constructions and signal flow of new CSs are given to describe the processes. Through the cascade operation, new CSs own more system parameters and expanded chaos areas. Besides, the maximum Lyapunov exponent is multiplied with the cascade time increasing, which means better chaotic performances. Detailed dynamic comparisons are explored to illustrate the improvements of CSs.

The rest of this paper is organized as follows. In Section 2, a DM model and its chaotic map are proposed and the corresponding i–v curves are given. In Section 3, the cascade DMCMs are established, and the dynamic comparisons between the seed map and CSs map are explored. In Section 4, the proposed chaotic systems are implemented. Finally, conclusions of the paper are summarized in Section 5.

2. The DM model and the seed chaotic map

2.1. The DM model

In terms of the definition of CM,[1] an ideal charge-controlled memristor can be defined as

$$\begin{cases} v(t) = M(q)i(t), \\ \dfrac{\mathrm{d}q(t)}{\mathrm{d}t} = i(t), \end{cases} \tag{1}$$

where $v(t)$ and $i(t)$ represent the voltage and input current through the memristor, respectively. $q(t)$ stands for a charge variable and $M(q)$ is the memristance function.

According to Euler difference method,[33] the CM in Eq. (1) can be transformed into

$$\begin{cases} v_n = M(q_n)i_n, \\ q_{n+1} = q_n + ki_n, \end{cases} \tag{2}$$

where v_n, q_n, and i_n represents the values of the n-th iteration of $v(t)$, $q(t)$, and $i(t)$.

The equation $q_{n+1} = q_n + ki_n$ can be deduced

$$\begin{cases} q_2 = q_1 + ki_1, \\ q_3 = q_2 + ki_2, \\ \ldots, \\ q_n = q_{n-1} + ki_{n-1}. \end{cases} \tag{3}$$

Therefore, q_n can be derived as

$$q_n = q_1 + k\sum_{j=1}^{n-1} i_j. \tag{4}$$

Thus, equation (1) can be converted into

$$v_n = M\left(q_1 + k\sum_{j=1}^{n-1} i_j\right) i_n. \tag{5}$$

It can be found that the current state of the DM depends on all of the past states.

In Ref. [36], a DM model was proposed as $M(q_n) = q_n^2 - 1$. Inspired by this model, we assume the DM model as $M(q_n) = u(aq_n^2 + b)$, then its characteristics can be described as follows:

$$\begin{cases} v_n = u(aq_n^2 + b)i_n, \\ q_{n+1} = q_n + ki_n, \end{cases} \tag{6}$$

where u, a, b, and k are system parameters.

Selecting parameters as $a = 1.5$, $b = -1$, $u = 1.76$, and $k = 1$, different pinched hysteresis loops are given in Fig. 1 by applying the discrete current source $i_n = I_{\mathrm{m}}\sin(\omega n)$. For different amplitudes I_{m} and frequencies ω, the hysteresis loops are always pinched at the origin. The lobe area of the hysteresis loop decreases as the frequency ω increases. These features are similar to those of CMs.

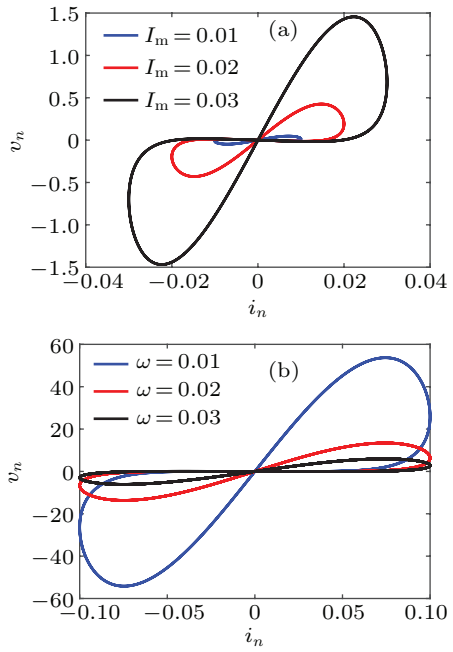

Fig. 1. The pinched hysteresis loops of the DM by applying (a) $i_n = I_{\mathrm{m}}\sin(0.01n)$ with $I_{\mathrm{m}} = 0.01$, 0.02 and 0.03; (b) $i_n = 0.1\sin(\omega n)$ with $\omega = 0.01$, 0.02, 0.03.

2.2. The DM-based seed map

Based on the above-mentioned system (6), a DMCM was reported in Ref. [36], which can be constructed as follows: denote i_n of the DM as the input for the n-th iteration map and v_n as the output and the next input of the iteration, then a two-dimensional (2D) memristive map can be described as[36]

$$\begin{cases} x_{n+1} = u\left(aq_n^2 + b\right)x_n, \\ q_{n+1} = q_n + kx_n. \end{cases} \tag{7}$$

The corresponding schematic structure is plotted as Fig. 2, where we treat this 2D map as $f_x(x_n, q_n)$. This seed map was treated as a normal chaotic map. Then the signal q_n is no longer regarded as the internal variable, but a signal that can be obtained as output. When the parameters are set as

$a = 1.5$, $b = -1$, $k = 1$, and $u = 1.76$ with initial value of $(x(1), q(1)) = (-0.1,\ 0.1)$, the numerical simulations of DMCM are plotted in Fig. 3. In this case, the Lyapunov exponents are calculated as $LE_1 = 0.2302$ and $LE_2 = 0.0985$. Thus, this map is hyperchaotic which will be used as a seed map for the cascade.

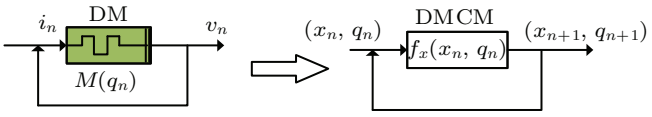

Fig. 2. The schematic structure of DMCM.

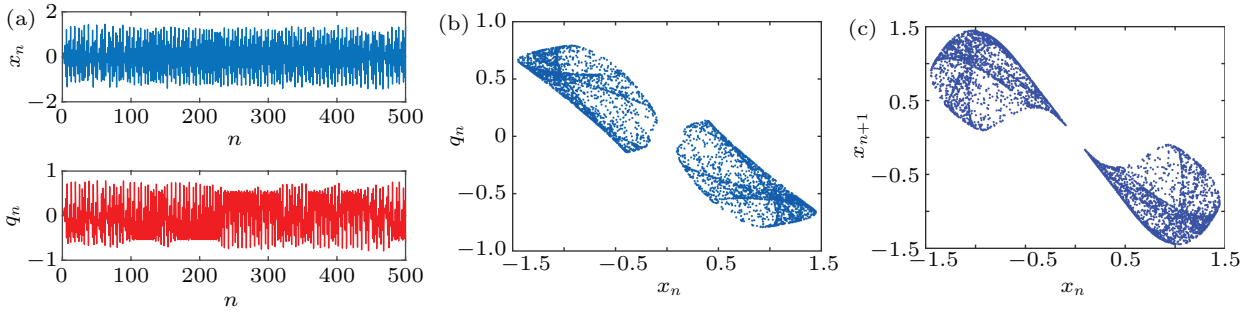

Fig. 3. Numerical simulations of DMCM (7): (a) iterative sequences of x_n, q_n, (b) phase portrait of x_n–q_n, (c) attractor of f_x.

3. The cascade DMCMs and dynamic comparisons

3.1. The cascade method of DMCMs

Motivated by the cascade structure in electronic circuits, the above-mentioned DMCM seed map can be utilized to cascade to construct more complex systems. Any number of DMCMs can be connected in series as shown in Fig. 4 to construct a new CS. Each DMCM sends its output to the latter until the last DMCM feeds its output back to the first one. Some cascade examples are given below.

3.2. Cascade with two DMCMs

To demonstrate the proposed method, the simplest CS can be constructed from the seed map as shown in Fig. 5(a), where two DMCMs $f_x(x_n, q_n)$ and $f_y(y_n, q_n^*)$ cascade with each other. The first seed map sends the outputs $(x_{n+1},\ q_{n+1})$ to the second map as the input signal, while the second map feeds back its outputs (y_{n+1}, q_{n+1}^*) to the input of the first. The detailed signal flow diagram of CS is described as shown in Fig. 5(b).

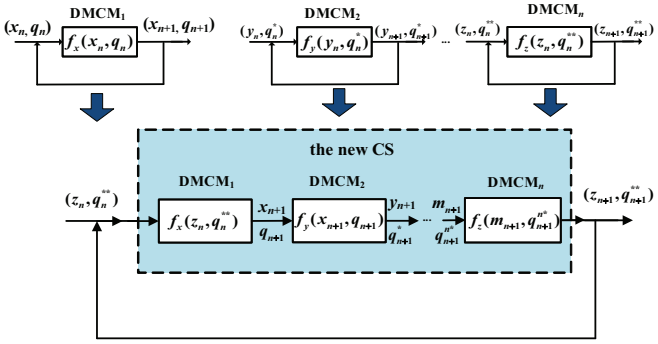

Fig. 4. The structure of multi-DMCM cascade.

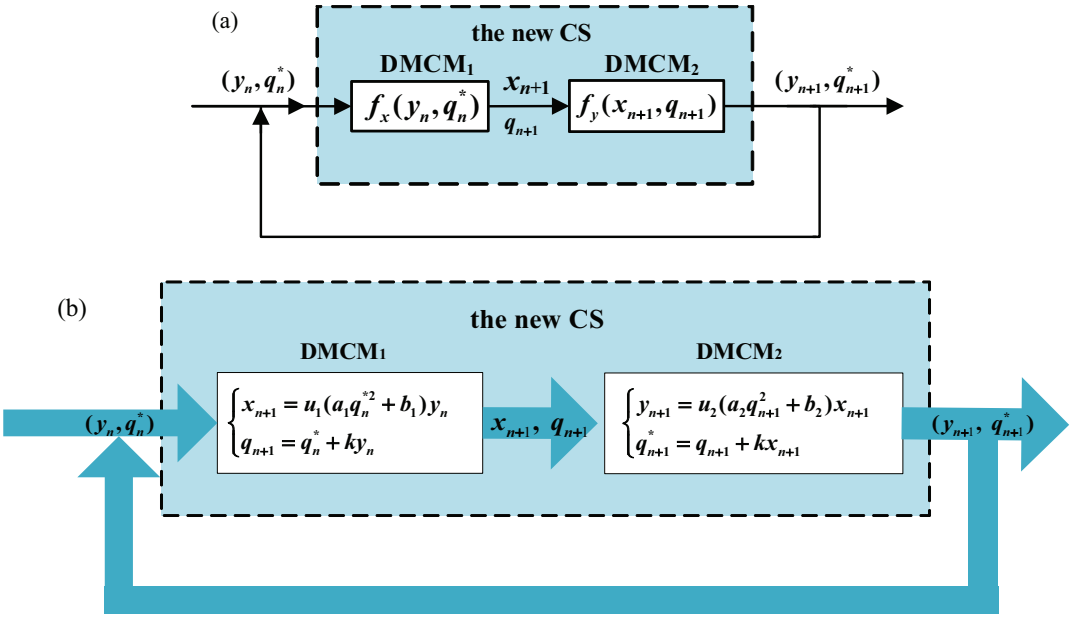

Fig. 5. The cascade of two DMCMs: (a) the structure chart and (b) the inner signal flow diagram.

Based on the signal flow diagram, the CS with two DMCMs can be described as

$$\begin{cases} y_{n+1} = u_2[a_2(q_n^* + ky_n)^2 + b_2][u_1\left(a_1 q_n^{*2} + b_1\right) y_n], \\ q_{n+1}^* = (q_n^* + ky_n) + k[u_1(a_1 q_n^{*2} + b_1) y_n]. \end{cases} \tag{8}$$

Obviously, the CS contains all parameters of its seed maps leading to a more complex structure. Setting parameters as the seed maps, there are $a_1 = a_2 = 1.5$, $b_1 = b_2 = -1$, $k = 1$, and $u_1 = u_2 = 1.76$. When the initial conditions are selected as $(-0.1, 0.1)$ and $(0.1, 0.1)$, the CS can generate chaotic oscillation and attractors as shown in Fig. 6.

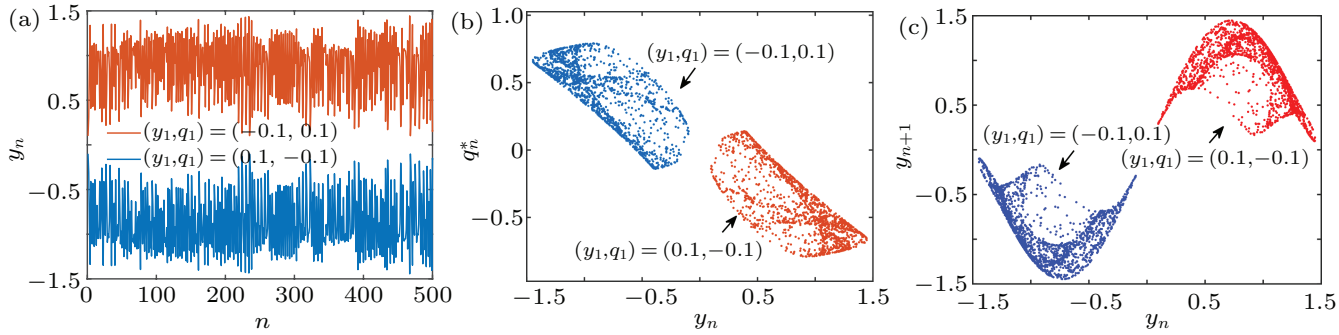

Fig. 6. Numerical simulations of CS (8): (a) iterative sequences of y_n, (b) phase portrait of y_n–q_n^*, (c) attractor of f_y.

3.3. Cascade with three DMCMs

Similarly, a CS with three DMCMs can be constructed as shown in Fig. 7(a), in which the DMCMs are defined as $f_x(x_n, q_n)$, $f_y(y_n, q_n^*)$, and $f_z(z_n, q_n^{**})$. The three DMCMs are connected in series. Each DMCM sends its output to the latter and the last DMCM feeds its output back to the first one. The corresponding internal signals of the CS are shown in Fig. 7(b).

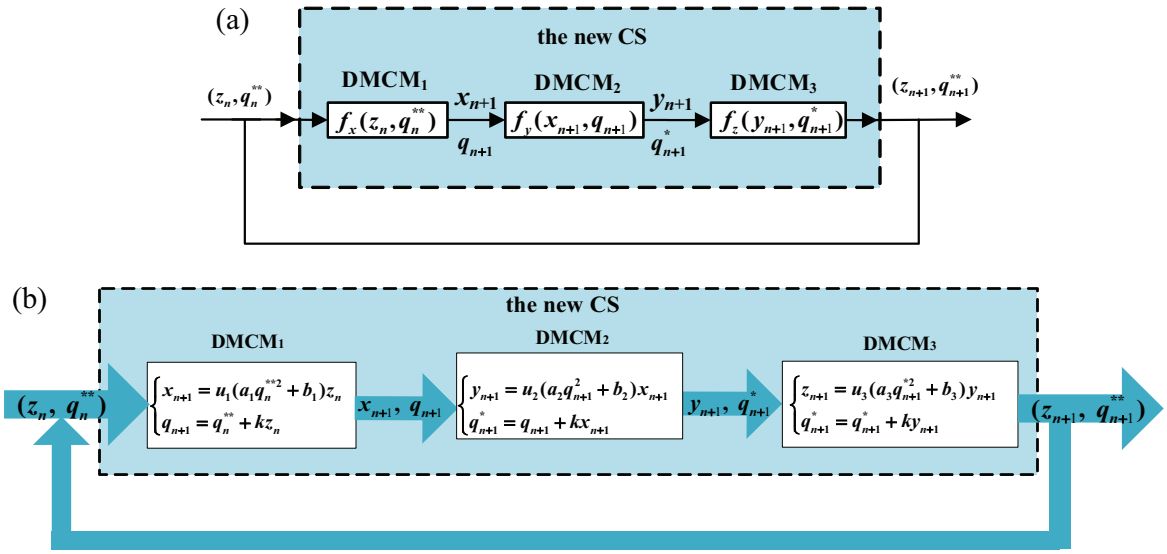

Fig. 7. The cascade of three DMCMs: (a) the structure chart and (b) the inner signal flow diagram.

Then the CS can be obtained as

$$\begin{cases} z_{n+1} = u_3\left(a_3\left[(q_n^{**} + kz_n)\right.\right. \\ \qquad \left. + k\left(u_1\left(a_1 q_n^{**2} + b_1\right) z_n\right)\right]^2 + b_3\Big) \\ \qquad \times u_2[a_2\left(q_n^{**} + kz_n\right)^2 + b_2]\left[u_1\left(a_1 q_n^{**2} + b_1\right) z_n\right], \\ q_{n+1}^{**} = (q_n^{**} + kz_n) + k\left[u_1\left(a_1 q_n^{**2} + b_1\right) z_n\right] \\ \qquad + ku_2[a_2\left(q_n^{**} + kz_n\right)^2 + b_2] \\ \qquad \times \left[u_1\left(a_1 q_n^{**2} + b_1\right) z_n\right]. \end{cases} \tag{9}$$

Setting parameters as $a_1 = a_2 = a_3 = 1.5$, $b_1 = b_2 = b_3 = -1$, $k = 1$, and $u_1 = u_2 = u_3 = 1.76$, the new CS also keeps chaotic state as shown in Fig. 8. Although the chaotic iterative trajectories and phase diagram z_n–q_n^{**} are similarly with the seed map (Figs. 3(a) and 3(b)), the system attractors are totally different, which means the change of the inner topology.

3.4. Dynamic comparisons

Chaos-cascade can significantly enlarge the maximum Lyapunov exponent and enhance the complexity of dynamic characteristics, which had been reported in previous researches.[26,27] In this case, since the seed DMCM is chaotic, their CSs also may have better dynamic features.

Taking $a_1 = 1.5$, $b_1 = -1$, and $k = 1$ in seed map (7), with initial value of $(-0.1, 0.1)$, the bifurcation diagram with respect to u_1 is shown in Fig. 9(a). The chaotic region of the seed system is mainly distributed in $u_1 \in (1.65, 1.85)$. For CSs (8) and (9), since the cascade operation increases the system parameters, the two CSs have more bifurcation variables and parameter configurations. Let parameters be the set of $a_1 = a_2 = a_3 = 1.5$, $b_1 = b_2 = b_3 = -1$, and $k = 1$. The corresponding bifurcation graphs of u_1, u_2, and u_3 are displayed in Figs. 9(b)–9(f). Obviously, the more system parameters provide the possibility for flexible parameter configurations. With appropriate parameters, the CSs have the larger chaotic areas than the seed map. The more cascade times, the larger chaotic areas of the system.

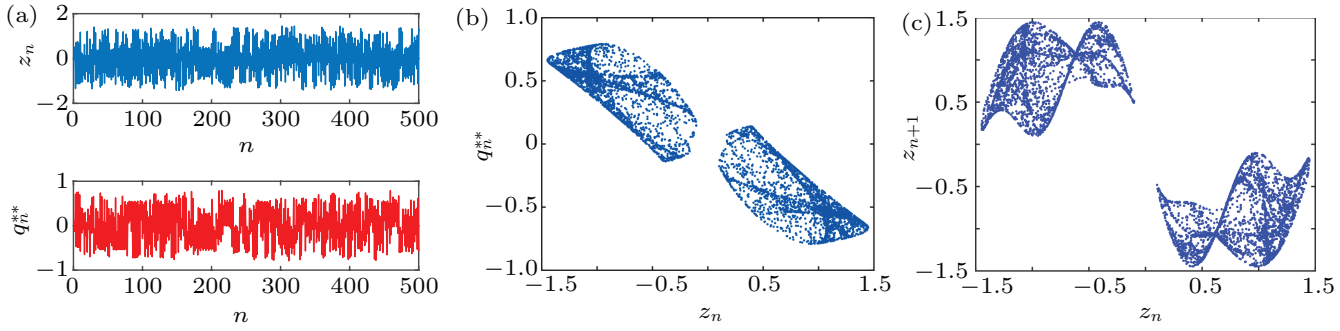

Fig. 8. Numerical simulations of CS (9): (a) iterative sequences of z_n and q_n^{**}, (b) phase portrait of z_n–q_n^{**}, (c) attractor of f_z.

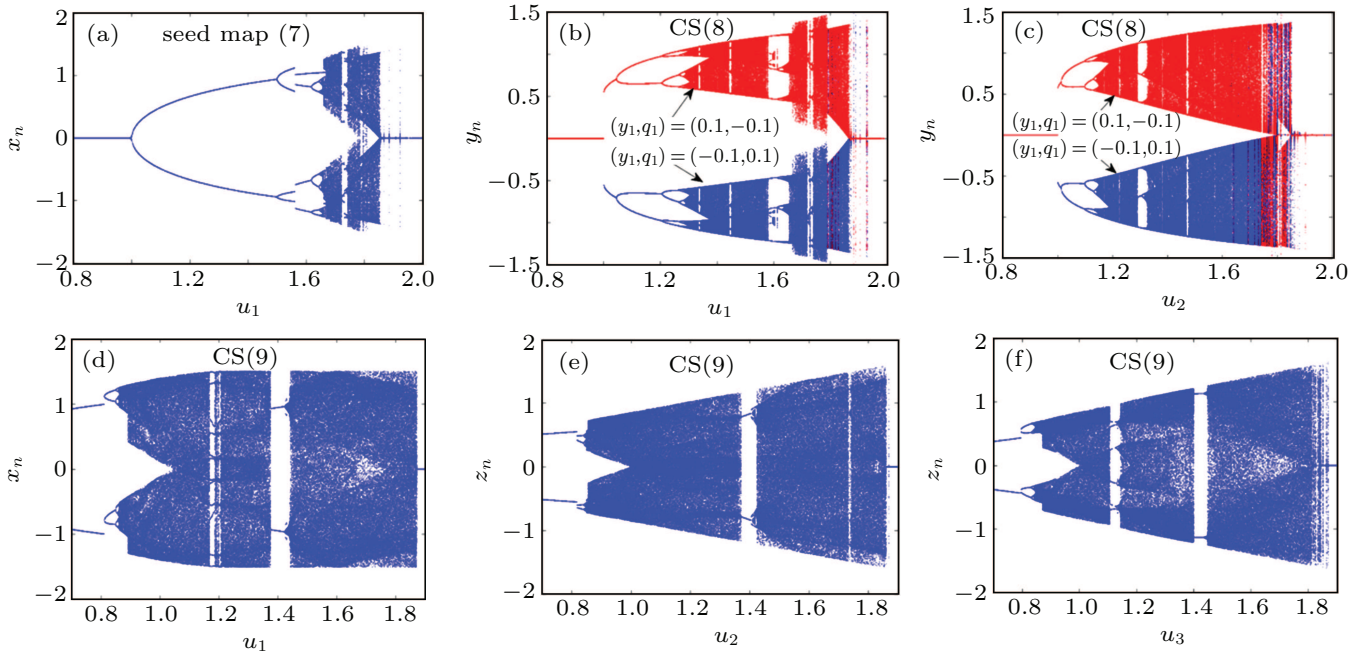

Fig. 9. The bifurcation diagrams of (a) seed map (7), (b) CS (8) with $u_2 = 1.76$, (c) CS (8) with $u_1 = 1.86$, (d) CS (9) with $u_2 = 1.76$ and $u_3 = 1.83$, (e) CS (9) with $u_1 = 1.83$ and $u_3 = 1.83$, (f) CS (9) with $u_1 = 1.76$ and $u_2 = 1.86$.

As mentioned above, the more system parameters mean the more parameter configurations, which may increase the chaotic parameter space. The expanded chaotic areas can be indicated from the dynamic maps, as shown in Figs. 10(a)–10(c), where the system initial values are all set as $(-0.1, 0.1)$. In these dynamic maps, the states of systems can be divided into five situations as the parameters change, namely fixed point (yellow color), period (cyan color), chaos (blue color), hyperchaos (black color), and divergence (red color). From the bottom left corner of dynamic maps, the two CSs all start from fixed point to periodic state via bifurcation, and jump into chaotic or hyperchaotic state through period doubling bifurcation. Then the system orbits turn to periodic state again from the reverse period-doubling bifurcation route, and finally move infinity as the parameters increase. Some typical system orbits are described in Fig. 10(d) for clearly displaying the variation of system states.

Compared with CSs (8) and (9), the chaotic and hyperchaotic areas with respect to u_1 and u_2 obviously become larger as the time of cascade increases. Because of cascade effect, the new parameter configuration u_1–u_3 emerges in CS (9). This new configuration brings new chaotic parameter space as shown in Fig. 10(c). Thus, new CSs own better performances in terms of chaotic dynamics.

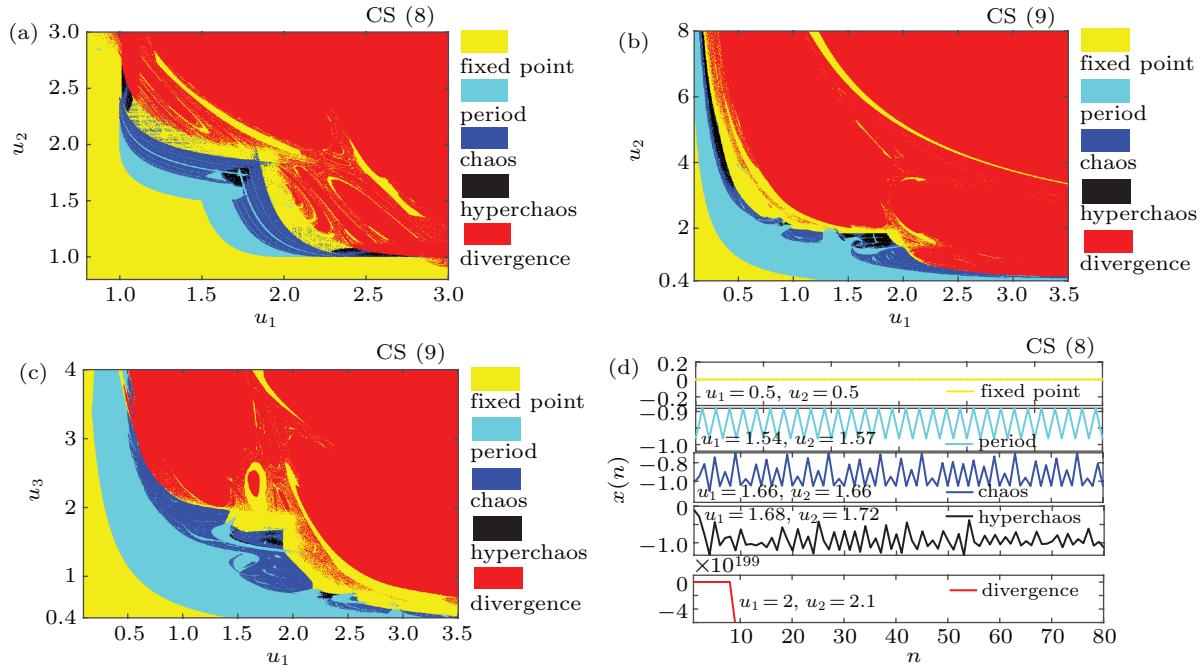

Fig. 10. Dynamic maps with respect of (a) u_1–u_2 in CS (8), (b) u_1–u_2 in CS (9), (c) u_1–u_3 in CS (9), and the typical system orbits of (d) CS (8).

Except for the expanded chaos areas, the CSs also own larger Lyapunov exponents. As shown in Fig. 11, the seed map owns the maximum Lyapunov exponent as $LE_{\max} = 0.3244$, while it increases to $LE_{\max} = 0.6704$ in CS (8) and $LE_{\max} = 0.9667$ in CS (9), respectively. The maximum Lyapunov exponent is multiplied compared with the seed map and increases with the cascade times. Since a larger Lyapunov exponent indicates more sensitive to changes of initial conditions, the CSs obviously own better statistical performance for the chaos generation.

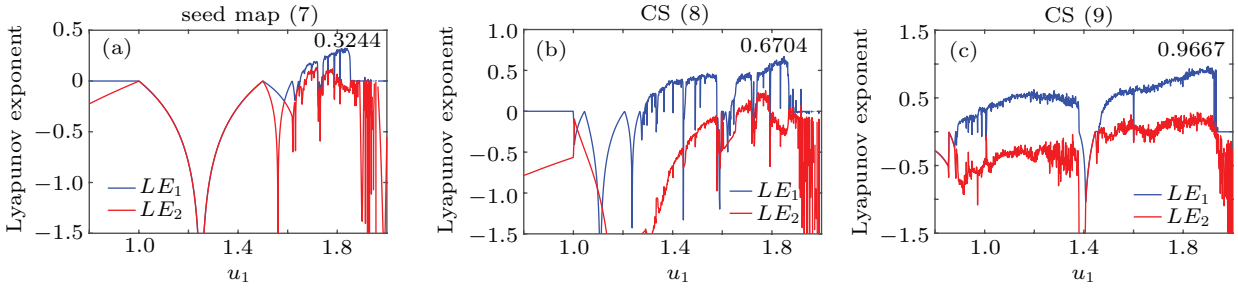

Fig. 11. The Lyapunov exponent spectra of the (a) seed map (7), (b) CS (8), (c) CS (9).

4. Hardware implementation

The proposed DM and its CSs are further implemented by digital signal processor (DSP) platform, where the core processing chip is TMS320C5509 and an 8-bit DA converter (TLC7528C) is used to convert numerical signals to analog voltage signals.

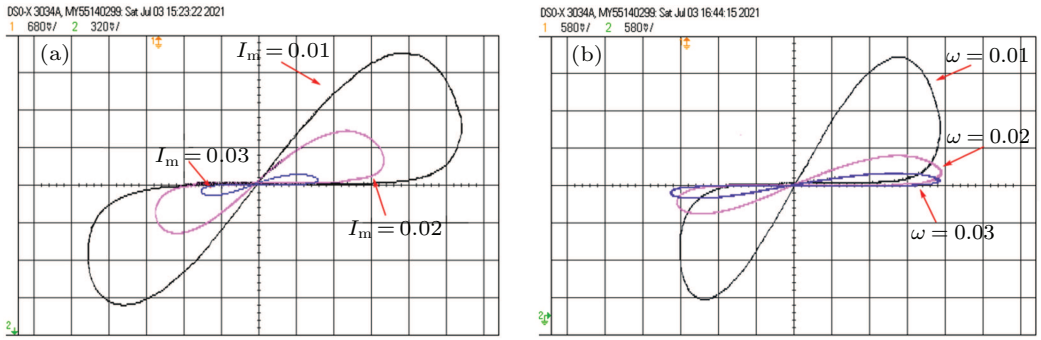

Fig. 12. The pinched hysteresis loops obtained by DSP: (a) $i_n = I_m \sin(0.01n)$ with $I_m = 0.1$, 0.2, and 0.3; (b) $i_n = 0.1\sin(\omega n)$ with $\omega = 0.01$, 0.02, and 0.03.

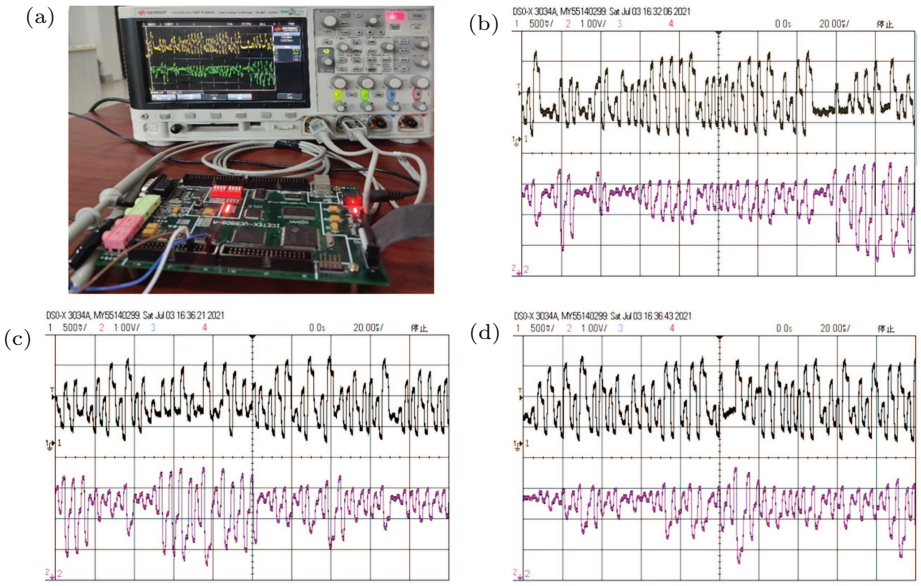

Fig. 13. DM chaotic sequences implemented on DSP platform. (a) Hardware device, and chaotic sequences generated by (b) seed map (7), (c) CS (8), (d) CS (9).

For different values of $I_{\rm m}$ and ω, the corresponding pinched hysteresis loops of the DM are obtained by the oscilloscope BSO-X3034A as shown in Figs. 12(a) and 12(b), respectively. These experimental results are consistent with the numerical simulations in shown Fig. 1.

Since the proposed DMCM and CSs are discrete systems, they can be naturally realized by digital platforms. Set parameters as $a_1 = a_2 = a_3 = 1.5$, $b_1 = b_2 = b_3 = -1$, $u_1 = u_2 = u_3 = 1.76$, and $k = 1$. The seed map (7), CSs (8) and (9) can generate chaotic sequences in the range of $(-1.6, 1.6)$. These sequences need to be converted and scaled up to the range of (0, 255) to adapt the 8-bit DA converter. The final experimental device and results are displayed in Fig. 13. It can be concluded that the generated chaotic sequences prove the feasibility of hardware implementation of DM chaotic maps.

5. Conclusion

In this paper, motivated by the cascade structure in electronic circuits, a DMCM is used as a seed map to construct CSs. Any number of the seed map can be connected in series to design new CSs. Compared with the seed map, these new CSs have more parameters and extended chaotic parameter space. As the times of cascade increases, the maximum Lyapunov exponent of CSs also significantly increases. Finally, the proposed systems are implemented on DSP platform. The experimental results indicate these new CSs can be used to generate pseudo-random sequences and applied to encryption fields.

References

[1] Chua L 2014 *Semicond. Sci. Tech.* **29** 104001
[2] Gu W Y, Wang G Y, Dong Y J and Ying J J 2020 *Chin. Phys. B* **29** 110503
[3] Lai Q, Wan Z Q, Kengne L K, Kuate P D K and Chen C Y 2021 *IEEE T. Circuits-II* **68** 2197
[4] Deng Y and Li Y X 2021 *Chaos* **31** 043103
[5] Xue W H, Ci W J, Xu X H and Liu G 2020 *Chin. Phys. B* **29** 048401
[6] Zhou Y, Hu X F, Wang L D and Duan S K. 2021 *Sci. China-Inform. Sci.* **64** 160408
[7] Sahu D P, Jetty P and Jammalamadaka S N 2021 *Nanotechnol.* **32** 155701
[8] Parit A K, Yadav M S, Gupta A K, Mikhaylov A and Rawat B 2021 *Chaos Soliton. Fract.* **145** 110818
[9] Ushakov Y, Balanov A and Savel'ev S 2021 *Chaos Soliton. Fract.* **145** 110803
[10] He S B, Sun K H and Wu X M 2020 *Phys. Scr.* **95** 035220
[11] Shi Q Y, Huang X, Yuan F and Li Y X 2021 *Chin. Phys. B* **30** 020507
[12] Gu W Y, Wang G Y, Dong Y J and Ying J J 2020 *Chin. Phys. B* **29** 110503
[13] Chen J J, Yan D W, Duan S K and Wang L D 2020 *Chin. Phys. B* **29** 110504
[14] Ouannas A, Khennaoui A A, Momani S, Pham V T and El-Khazali R 2020 *Chin. Phys. B* **29** 050504
[15] Wu H G, Bao H, Xu Q and Chen M 2019 *Complexity* **2019** 3687635
[16] Wang F P and Wang F Q 2020 *Chin. Phys. B* **29** 058502
[17] Wu H G, Ye Y, Chen M, Xu Q and Bao B C 2019 *IEEE Access* **7** 145022
[18] Hua Z Y and Zhou Y C 2021 *IEEE T. Syst. Man Cy-s.* **51** 3713
[19] Li C Q, Lin D D, Lu J H and Hao F 2018 *IEEE Multimedia* **25** 46
[20] Zhao C and Wu B 2021 *Chin. Phys. Lett.* **38** 030502
[21] Zhang J C, Ren W K and Jin N D 2020 *Chin. Phys. Lett.* **37** 090501
[22] Wu H G, Ye Y, Bao B C, Chen M and Xu Q 2019 *Chaos Soliton. Fract.* **121** 178
[23] Bao B C, Bao H, Wang N, Chen M and Xu Q 2017 *Chaos Soliton. Fract.* **94** 102
[24] Gu M Y, Wang G Y, Liu J B, Liang Y, Dong Y J and Ying J J 2021 *Int. J. Bifurcat. Chaos* **31** 2130018
[25] Bao B C, Zhu Y X, Ma J, Bao H, Wu H G and Chen M 2021 *Sci. China-Technol. Sci.* **64** 1107
[26] Yuan F, Li Y X and Wang G Y 2021 *Chaos* **31** 021102
[27] Yuan F, Deng Y, Li Y X and Chen G R 2019 *Chaos* **29** 053120
[28] Chua L O and Kang S M 1976 *Proc. IEEE* **64** 209
[29] Peng Y X, He S B and Sun K H 2021 *Results Phys.* **24** 104106
[30] Peng Y X, He S B and Sun K H 2021 *AEU-Int. J. Electron. Commun.* **129** 153539
[31] He S B, Sun K H, Peng Y X and Wang L 2020 *AIP Adv.* **10** 015332
[32] Peng Y X, Sun K H and He S B 2020 *Chaos Soliton. Fract.* **137** 109873
[33] Bao B C, Li H Z, Wu H G, Zhang X and Chen M 2020 *Electron. Lett.* **56** 769
[34] Li H Z, Hua Z Y, Bao H, Zhu L and Bao B C 2020 *IEEE Trans. Ind. Electron.* **68** 9931
[35] Deng Y and Li Y X 2021 *Chaos Soliton. Fract.* **150** 111064
[36] Bao H, Hua Z Y, Li H Z, Chen M and Bao B C 2021 *IEEE T. Circuits-I* **68** 4534